



Flexural behavior of reinforced concrete beams and prediction of failure stages

 Abudusaimaiti Kali^{1,2},  Zihao Wang^{1,2},  Alipujiang Jierula^{1,2,*}

¹College of Civil Engineering and Architecture, Xinjiang University, Urumqi, China

²Xinjiang Key Laboratory of Building Structure and Earthquake Resistance, Xinjiang University, Urumqi, China

*Correspondence: alp@xju.edu.cn

Abstract. Reinforced concrete (RC) beams are fundamental flexural members in engineering structures. The mechanisms of flexural failure and shear failure differ significantly and directly affect structural safety design. This study systematically investigates the mechanical responses of RC beams with two distinct reinforcement ratios under flexural failure and shear failure. A BP neural network model based on the Bayesian regularization algorithm is developed to predict the failure mode and load state of RC beams. Experimental results of flexural failure indicate that in RC beams, the tensile steel yields first (at a load of 60 kN, the steel strain reaches 1500 $\mu\epsilon$), followed by concrete crushing and the formation of a plastic hinge. The load-deflection curve exhibits a pronounced yield flow stage (deflection jumps from 10.10 mm to 15.15 mm), demonstrating ductile failure with early warning characteristics. In contrast, shear failure tests show that under a short shear span ratio, the beam achieves a higher load-carrying capacity (up to 140 kN, approximately 2.2 times that of the flexural beam) through an arch action. However, the failure is sudden and brittle: as the load increases from 120 kN to 140 kN, the deflection jumps by 4.75 mm, accompanied by a sharp increase in steel strain. Furthermore, the developed BP neural network model takes concrete strain as input and load as output. The regression values for training and testing are all close to 1 (0.994 and 0.996 for the flexural model; 0.999 and 0.998 for the shear model), with small mean square errors. The results demonstrate that the neural network model can predict the load and failure stage of RC beams with high accuracy, providing a reliable basis for engineering design against flexure and shear.

Keywords: reinforced concrete beams, flexural failure test, shear failure test, BP neural network, failure stage.

1. Introduction

Reinforced concrete (RC) beams are the most common flexural members in engineering structures. Their failure modes are mainly influenced by the shear-span ratio (λ), reinforcement ratio (ρ), and stirrup configuration. Flexural failure of the normal section typically manifests as crushing of concrete after yielding of the tensile reinforcement, providing good ductility and warning. In contrast, shear failure of the inclined section is often caused by the propagation of diagonal cracks leading to shear-compression or diagonal tension failure of concrete, characterized by suddenness. Accurately understanding these two failure mechanisms is crucial for structural safety design.

In terms of flexural behavior of the normal section, stress analysis and failure mechanisms based on fracture mechanics and long-term performance have been investigated [1]. Specifically, a fracture mechanics-based program was developed to assess the strength and crack resistance of RC beam elements [2]; a one-dimensional finite element framework incorporating nonlinear material behavior, damage mechanics, and time-dependent effects was proposed to predict the long-term flexural response of RC beams [1]; and the stress intensity factor under bending, involving fracture mechanics analysis of crack propagation, was examined [3].

The performance of beams under serviceability limit states has been investigated. Through finite element analysis, the contribution of the tension stiffening effect to the stiffness of beam

members after concrete cracking was examined [4]. Methods for estimating stress distribution and stiffness of continuous beams under serviceability limit states have also been studied [5].

Flexural behavior and analytical methods for specific beam types have been explored. The finite element method was utilized for ultimate load analysis of RC beams [6]. A comprehensive review of studies on the flexural behavior and design of RC beams strengthened with or using Fiber Reinforced Polymer (FRP) bars as reinforcement or replacement for steel bars has been provided [7].

In terms of the shear behavior of the inclined section, a unified design criterion for shear stress limits has been proposed. Through the design and testing of asymmetrically loaded reinforced concrete deep beams, this research aimed to establish an appropriate unified shear stress limit for RC beam design to simplify the design process and enhance safety [8]. A shear hinge model for analyzing the shear behavior of beams has been developed. This model, which belongs to the concentrated plasticity approach, is capable of capturing complex mechanisms such as shear-moment interaction, nonlinear stress-strain distribution across the section, and concrete softening, thereby providing an effective analytical tool for system-level structural performance assessment [7]. The application of the stress field method for deep beam design has been explored. Through analysis and experimentation, this research investigated the application of the stress field method in the analysis and design of deep beams (particularly those with low shear-span ratios and containing openings), addressing their specific shear mechanics problems [9].

This paper investigates and compares the mechanical responses of RC beams with different reinforcement configurations under two distinct failure modes, analyzes the mechanical response for each failure mode, and establishes models to predict the failure of reinforced concrete beams.

2. Materials and Methods

2.1 Test setup and materials

Figure 1 presents the detailed design drawings of the specimen, while Figure 2 shows the as-built photos.

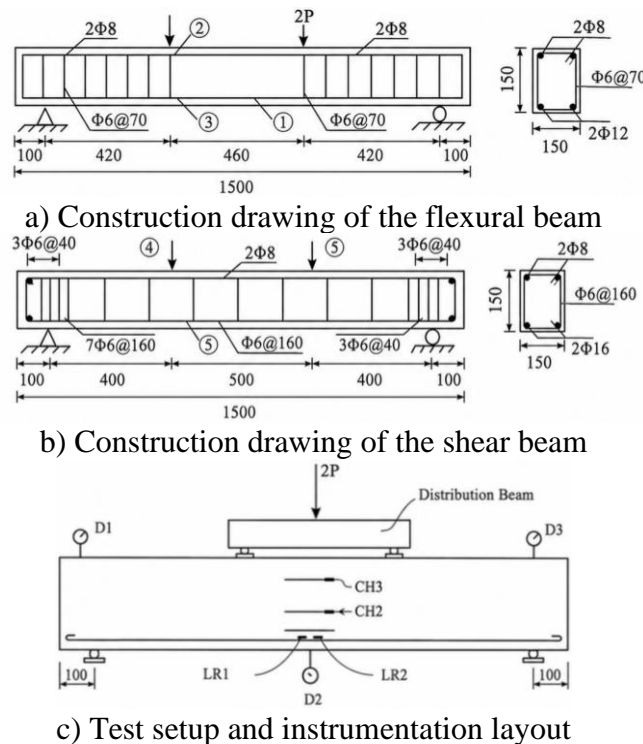


Figure 1 – Test specimens and experimental setup: D – dial gauges (for deflection); CH – strain gauges on the side face of the beam; CP – strain gauges on the top (compression zone) face of the beam; LR – strain gauges on the longitudinal reinforcement

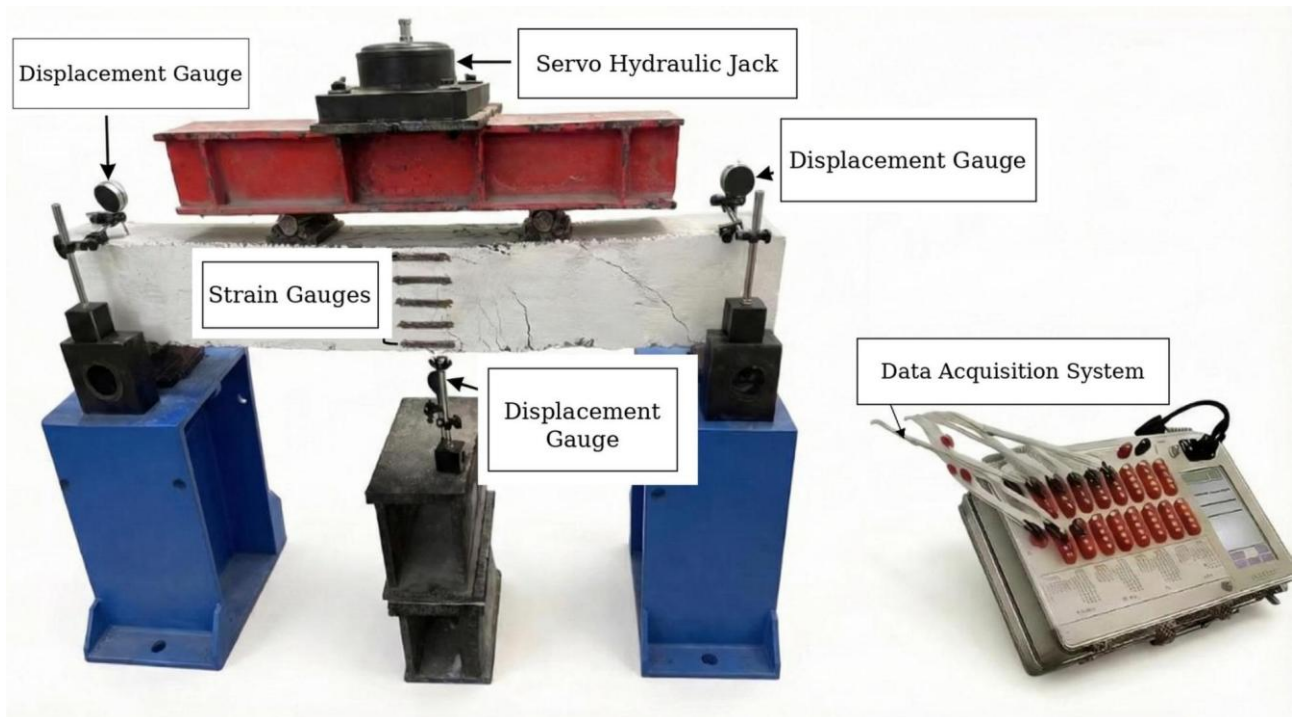


Figure 2 – Photograph of the experimental setup

The longitudinal reinforcement ratio was controlled between ρ_{\min} and ρ_{\max} . Concrete of grade C30 was used with a mix ratio of 0.44:1:1.328:3.1 (water:cement:sand:coarse aggregate). The specimen configuration for the shear failure test of the supported RC beam is also illustrated. The longitudinal reinforcement ratio similarly satisfied $\rho_{\min} \leq \rho \leq \rho_{\max}$. The concrete strength grade was C30 (mix ratio consistent with the under-reinforced beam). HRB400 steel bars were used for longitudinal reinforcement, and HPB300 bars were used for hanger bars. The detailed information on the test specimens is provided in Table 1. The major chemical compositions of the cement are presented in Table 2.

Table 1 – Details of test specimens

Category	Parameter	Test 1: Under-reinforced beam (flexural failure-normal section)	Test 2: Shear-critical beam (shear failure-diagonal section)
Geometry	Width b (mm)	150	150
	Height h (mm)	200	200
	Clear Span L (mm)	1500	1500
	Concrete Cover c(mm)	25	25
Concrete	Strength Grade	C 30	C 30
	Mix ratio (water: cement: sand: aggregate)	0.44:1:1.328:3.1	0.44:1:1.328:3.1
	Compressive strength f_{cu} (MPa)	35.0	35.0
	Elastic Modulus E_c (MPa)	3.10×10^4	3.10×10^4
Reinforcement configuration	Longitudinal rebar	HPB300, $\Phi 12$	HRB400, $\Phi 16$
	Compression bars	HPB300, $\Phi 8$	HPB300, $\Phi 8$
	Stirrups	HPB300, $\Phi 6 @ 70\text{mm}$	HPB300, $\Phi 6 @ 160\text{mm}$ HPB300, $\Phi 6 @ 40\text{mm}$
Material Properties	Yield Strength f_y , MPa	340	450
	Elastic Modulus E_s , MPa	2.10×10^5	2.00×10^5
Curing	Conditions	Standard curing, 28 days	Standard curing, 28 days
Specimens	Quantity	1	1
Test Protocol	Replication	Each group replicated twice Total: 4 specimens.	Each group replicated twice Total: 4 specimens.

Table 2 – Chemical composition of cement [10]

Oxide	CaO	SiO ₂	Al ₂ O ₃	SO ₃	Fe ₂ O ₃	MgO	K ₂ O	TiO ₂	P ₂ O ₅	Na ₂ O
Cement	63.00	20.95	5.39	4.52	3.21	1.34	0.77	0.39	0.19	0.07

A synchronous hydraulic control system, equipped with corresponding hydraulic rams, was used for loading. The setup included a static resistance strain indicator, load cells, dial gauges with magnetic bases, magnifying lenses with scales, steel tape measures, and other related auxiliary tools. The specifications of the equipment used in the tests are presented in Table 3.

Table 3 – Test equipment specifications

Equipment (Model)	Manufacturer
Static strain testing system (DH3818Y)	Jiangsu Donghua Testing Technology Co., Ltd. (Jingjiang, China)
Mechanical dial indicator (321-135W)	Guilin Guanglu Digital Measuring & Control Co., Ltd. (Guilin, China)
Resistance strain gauges (BX120-80AA / BX120-4AA)	Zhejiang Huangyan Test Instrument Factory (Taizhou, China)
Spoke-type load cell (LC.P-500)	Hangzhou Bangwei Electromechanical Control Engineering Co., Ltd. (Hangzhou, China)
Servo actuator (MAS-500/500Q)	
Multi-channel electro-hydraulic servo coordination loading system	

2.2 Test content and key points

The tests aimed to analyze the mechanical performance of the beams under load, assess their strength safety margin, measure crack widths, deflections at different load stages, and crack development status. Simultaneously, strain values and their variation trends in critical sections were obtained to study the law of member stiffness variation with load [11].

Given that beam test loads are typically large, multi-point loading often employs a synchronous hydraulic loading system. The load arrangement should follow the design requirements. If actual conditions differ, adjustments are made based on the principle of equivalent load to ensure that the internal force distribution under the test load is essentially consistent with the design internal forces, with equal internal force values at key sections.

The loading process was applied incrementally. Five load levels were used up to the standard load. The self-weight of the specimen and the weight of the loading equipment were included in the initial load. The appearance and development of cracks were recorded visually. Crack widths were measured using a scaled magnifying lens. Under the standard load, the maximum crack widths on both the normal section and the inclined section needed to be measured simultaneously. The flexural crack width was taken as the maximum value at the level of the reinforcement (including the bottom and side faces). Diagonal cracks were measured at their widest point. A schematic diagram of the crack pattern at each load level was drawn on the specimen, annotated with the corresponding load level and crack width.

To accurately determine the cracking load, before loading to the estimated cracking load, each load increment was set at 5% of the standard load (P), and the occurrence of the first crack was closely observed. As failure approached, the failure characteristics were recorded, and the failure load value was determined.

2.3. Failure criteria

The specimen is considered to have failed, and the corresponding load is taken as the failure load, upon the occurrence of any of the following conditions: a) Failure of concrete in the compression zone; b) Fracture of the longitudinal tensile reinforcement; c) The deflection of the member reaches 1/50 of the span after the longitudinal tensile reinforcement yields or exceeds its yield strength; OR the maximum crack width at the location of the longitudinal tensile reinforcement reaches 1.5 mm.

The specimen is considered to have failed, and the corresponding load is taken as the failure load, upon the occurrence of any of the following conditions: a) The width of a diagonal web crack

reaches 1.5 mm, OR shear-compression failure of the concrete occurs at the tip of the diagonal crack; b) Diagonal compression failure of concrete along the inclined section; OR anchorage failure, such as slippage of the main tensile reinforcement at the ends; c) When determining the actual cracking load and failure load of the specimen, the self-weight of the specimen and the weight of loading equipment such as bearing plates and distribution beams acting on the specimen must be included.

2.4. Test procedure

The test procedure was as follows: a) Calculate the load increments based on 20% of the standard load P . The initial load includes the self-weight of the specimen and the weight of equipment like distribution beams; b) Attach strain gauges according to specifications, perform moisture-proof treatment, arrange wiring, and install deflection measurement devices; c) Conduct pre-loading for 1-3 levels, check instrument functionality, and troubleshoot. The pre-load value should be lower than the cracking load; d) During formal loading, the self-weight and loading equipment weight constitute the first load level. If this does not reach the first incremental load level, supplement with additional external load; e) Maintain each load level for 2-5 minutes. Read and record data during the holding period; f) Closely monitor the operation status of instruments and the loading system throughout the test. Record crack development and the final failure mode in detail. Figure 3 shows the crack pattern and failure mode.

3. Results and discussion

3.1 Comparative response of beams under flexural and shear failure

The experimental results show clear differences between the flexural and shear responses of the reinforced concrete beams. Although both specimens were tested under vertical loading, their crack development, load-displacement behavior, reinforcement strain response, and failure mechanisms were substantially different. The flexural beam exhibited a ductile failure mode governed mainly by tensile reinforcement yielding and subsequent concrete crushing, whereas the shear beam showed a more sudden and brittle failure mode controlled by diagonal cracking in the shear span. The observed failure patterns are presented in Figure 3.

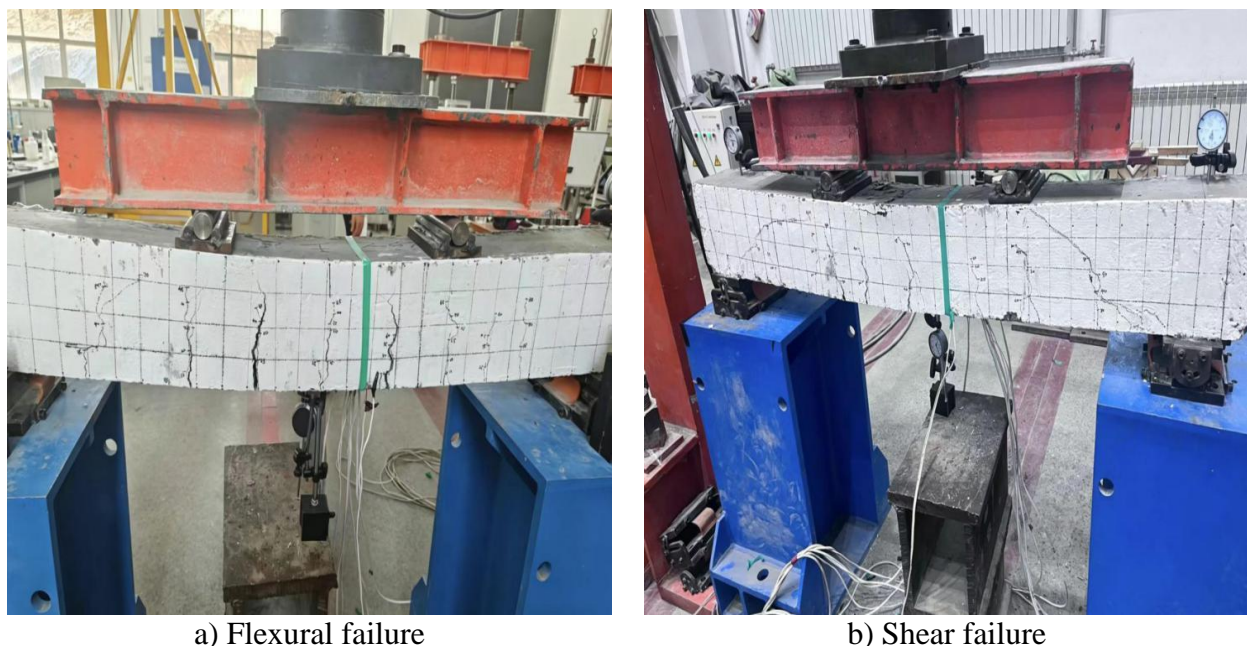


Figure 3 – Failure modes of specimens

In the flexural beam, vertical cracks developed mainly in the constant-moment region and propagated upward from the tensile zone, as shown in Figure 3a. This crack pattern is typical of

flexural failure, where tensile stresses first cause cracking at the bottom of the beam, followed by progressive stiffness reduction and yielding of the longitudinal reinforcement. The final damage mode indicates that the beam was able to undergo significant deformation before failure. In contrast, the shear beam developed dominant inclined cracks in the shear span, as shown in Figure 3b. These diagonal cracks propagated rapidly toward the loading point and support region, indicating that the inclined section controlled the failure. Compared with the flexural specimen, the crack pattern of the shear specimen was less gradual and more localized, which is consistent with the brittle nature of shear failure.

The difference between the two failure mechanisms is also reflected in the load-displacement curves shown in Figure 4.

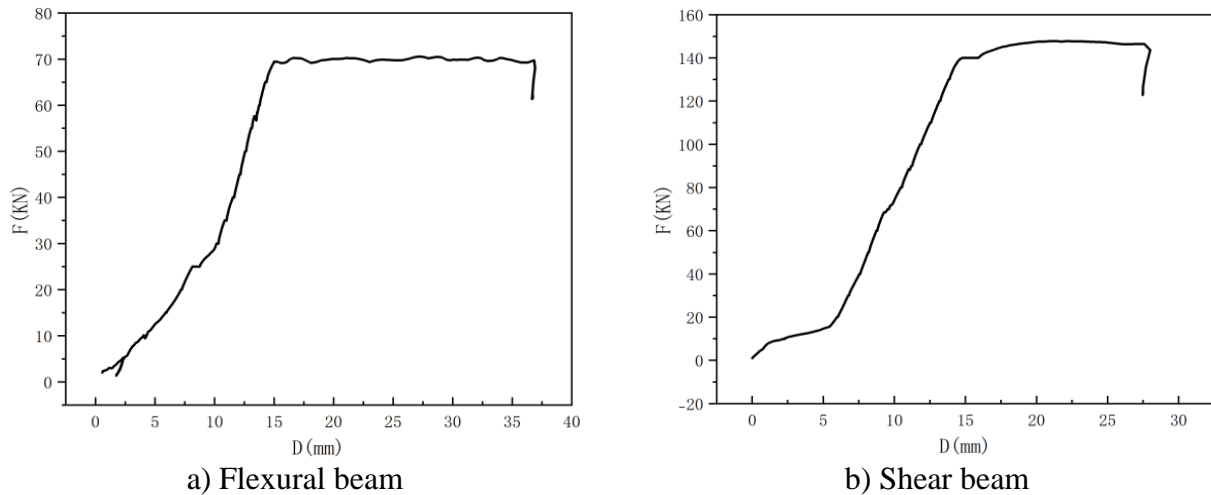


Figure 4 – Load-displacement curves

For the flexural beam, the curve in Figure 4a shows three main stages. At the initial stage, the load increased with only a small increase in displacement, indicating relatively high initial stiffness before significant cracking. As the load increased, flexural cracks developed in the tensile zone, reducing the effective stiffness of the section and causing a more rapid increase in displacement. Near the peak load, the curve became almost horizontal, showing that the beam had entered the yielding stage. When the load increased from approximately 60 kN to 63 kN, the displacement increased sharply from about 10.10 mm to 15.15 mm. This response indicates that the tangent stiffness had decreased significantly and that a plastic hinge was forming in the critical flexural region. Therefore, the flexural beam displayed ductile behavior with clear deformation development before failure.

The shear beam showed a different load-displacement response, as presented in Figure 4b. Its peak load reached approximately 140 kN, which was about 2.2 times greater than the peak load of the flexural beam. This higher load-carrying capacity can be attributed to the short shear-span behavior and the development of arch action, where part of the load is transferred directly through a compression strut between the loading point and the support. However, the higher capacity was accompanied by lower ductility. At the initial stage, the shear beam showed high stiffness and limited displacement growth. With further loading, diagonal cracks developed, and the stiffness gradually decreased. In the final stage, when the load increased from approximately 120 kN to 140 kN, the displacement increased from about 10.36 mm to 15.11 mm. This sudden displacement increase over a relatively small load interval indicates rapid stiffness loss and unstable diagonal crack propagation. Thus, unlike the flexural beam, the shear beam failed in an abrupt and brittle manner.

The steel stress-strain curves further confirm the different failure mechanisms of the two specimens. For the flexural beam, Figure 5a shows that the tensile reinforcement initially remained within the elastic range, with a nearly linear stress–strain relationship. As the load approached approximately 60 kN, the steel strain reached about 1500 $\mu\epsilon$, corresponding to the yield strain of HPB300 reinforcement. After yielding, the steel strain increased rapidly while the load increased only

slightly. This confirms that the tensile reinforcement yielded before final concrete crushing, which is the expected failure sequence for an under-reinforced flexural member. The reinforcement response is therefore consistent with the ductile load-displacement behavior observed in Figure 4a.

For the shear beam, the steel stress-strain response in Figure 5b indicates a different process. The reinforcement response was approximately linear at lower load levels, but the strain increased more rapidly after diagonal cracking developed. The steel strain exceeded approximately $2000 \mu\epsilon$ at around 90 kN, indicating that the HRB400 reinforcement approached or reached the yield range. At the failure stage, the strain increased sharply, reaching values above $4000 \mu\epsilon$ in some measurements. This sudden increase suggests that, after the formation of major diagonal cracks, internal force redistribution became unstable and the reinforcement was rapidly engaged in resisting shear-induced deformation. Therefore, the strain response of the shear beam supports the conclusion that its failure was sudden and governed by diagonal crack propagation rather than gradual flexural yielding.

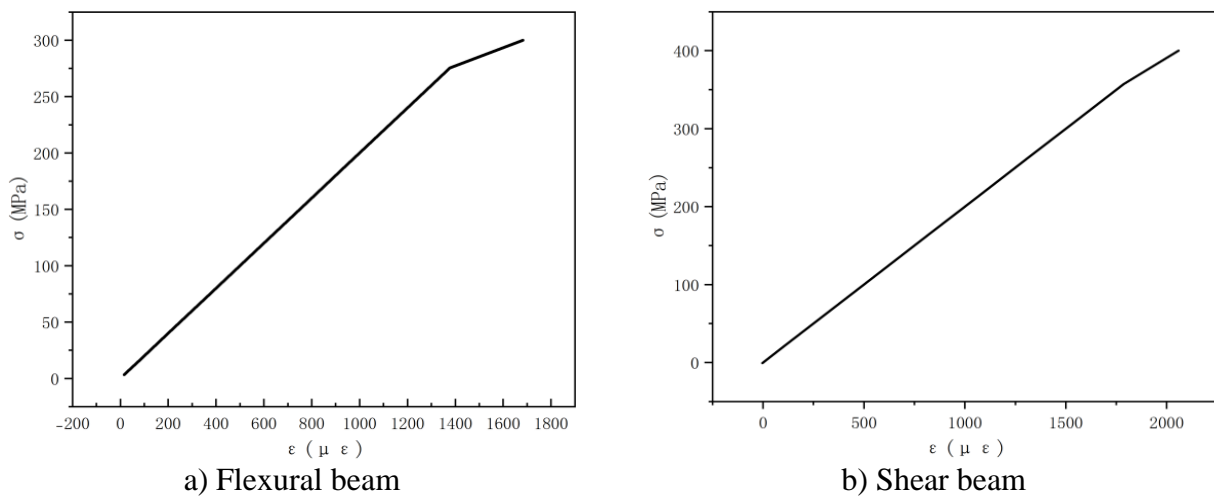


Figure 5 – Stress-strain curves of the steel reinforcement

The concrete strain distribution and neutral axis movement also provide important evidence for the different responses of the two beams. In the flexural beam, the neutral axis shifted upward gradually as the load increased. This occurred because tensile cracks propagated from the bottom of the beam toward the compression zone, reducing the effective depth of the uncracked concrete section. As a result, the compression zone became smaller, and the compressive strain in the upper concrete fibers increased. This gradual movement of the neutral axis is consistent with flexural crack development and the formation of a plastic hinge after reinforcement yielding.

In the shear beam, the neutral axis movement was less stable near failure because diagonal cracking significantly disturbed the strain distribution across the section. At approximately 120 kN, the measured concrete strains of $-560 \mu\epsilon$ at Gauge 1, $-328 \mu\epsilon$ at Gauge 2, and $144 \mu\epsilon$ at Gauge 3 indicate that the neutral axis was located near Gauge 2. At 140 kN, the strain at Gauge 2 decreased to approximately $-14 \mu\epsilon$, while the strain at Gauge 3 increased to about $1116 \mu\epsilon$. This sharp change indicates a rapid upward shift of the neutral axis and a sudden redistribution of stresses caused by diagonal crack development. Such behavior shows that the assumption of a stable flexural strain distribution becomes less applicable as shear failure approaches.

Overall, the experimental results demonstrate that the flexural beam and the shear beam had fundamentally different failure characteristics. The flexural beam reached a lower peak load of approximately 63 kN but showed ductile behavior, including visible flexural cracking, yielding of the tensile reinforcement, large displacement development, and a clear warning before failure. In contrast, the shear beam reached a higher peak load of approximately 140 kN due to arch action, but its failure was sudden and brittle, with rapid diagonal crack propagation, abrupt displacement growth, and sharp reinforcement strain increase. Therefore, although the shear beam had a greater load-carrying capacity, its failure mode was more dangerous from a structural safety perspective. These results

confirm that reinforced concrete beam design should avoid brittle shear failure and should promote ductile flexural behavior wherever possible.

3.2 Prediction of failure stages using a neural network learning model

Artificial Neural Networks (ANNs) are information processing systems that simulate the biological neural networks of the human brain. They are powerful computational algorithms widely used in machine learning. An ANN consists of numerous interconnected nodes, which form the input layer, output layer, and hidden layers. Its functionality is highly dependent on the connections between these nodes. ANNs have been successfully applied to understand complex engineering problems and have demonstrated excellent performance [12].

The Backpropagation (BP) Neural Network is a type of ANN [13]. It employs supervised learning aimed at error minimization, and its algorithm is trained using the backpropagation method. In the BP algorithm, signals propagate forward during the learning process, while errors propagate backward. The structure of a BP network comprises at least three layers: an input layer, a hidden layer, and an output layer. The BP network learning model used in this study was constructed using the Neural Network Toolbox in MATLAB R2025b software. A process diagram of the BP network simulation model used in this study is provided in the corresponding Figure 6.

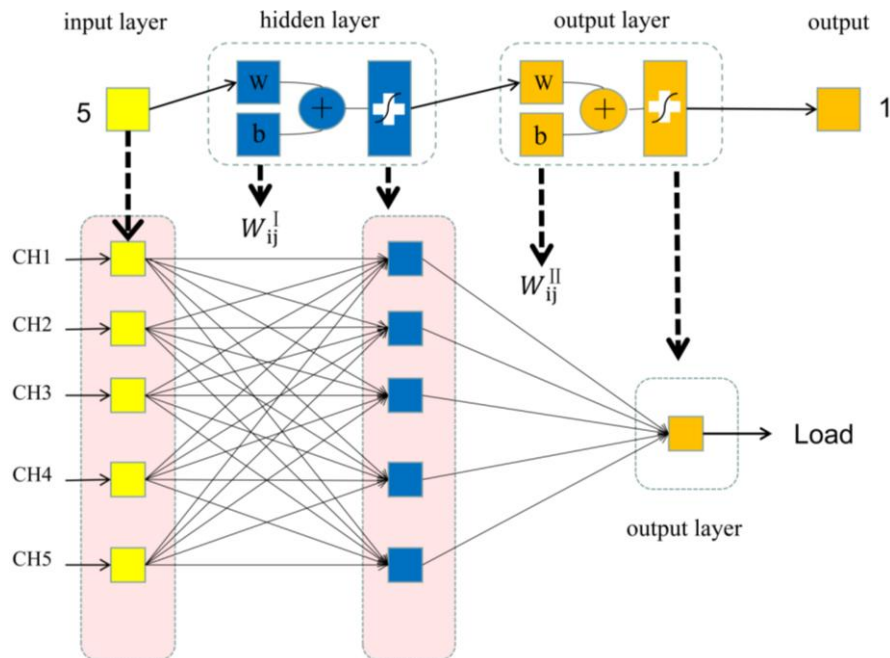


Figure 6 – Schematic of the three-layer BP neural network model

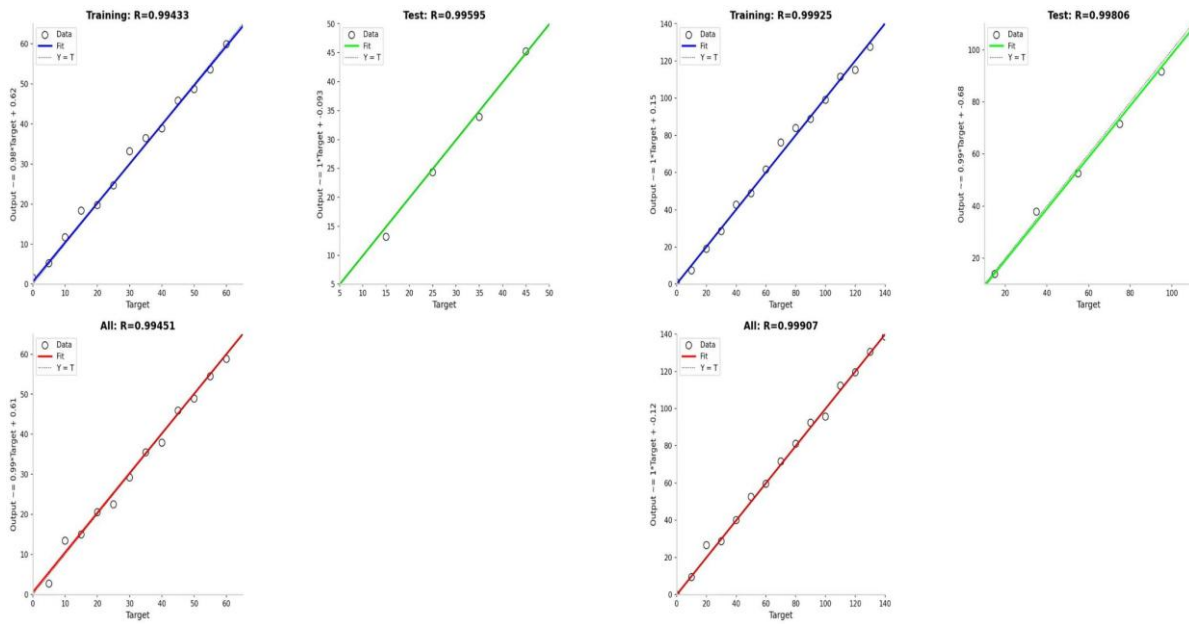
The input sample datasets were obtained from flexural failure tests and shear failure tests on simply supported, under-reinforced (beams with reinforcement ratio within the designed range) RC beams. The first dataset has a size of 6×28 (28 data entries, each containing 6 parameters). The second dataset has a size of 6×32 (32 data entries, each containing 6 parameters). The input variables are the strains in the concrete, and the output parameter is the load applied to the beam.

This study prioritized the use of the Bayesian Regularization algorithm. This selection was primarily based on the following two considerations: First, mechanical tests on concrete are characterized by small sample sizes. Data acquisition is costly, and the sample volume obtained from such tests is often limited. This makes the model highly susceptible to overfitting during training, meaning the model adapts too closely to random noise in the training data rather than the underlying physical principles. The Bayesian Regularization method effectively constrains the complexity of the neural network by introducing a regularization term, thereby enhancing its generalization capability. This ensures the model maintains reliable predictive performance even with unseen data. Second, robustness for engineering applications holds the highest priority. Compared to algorithms focused

merely on training speed, Bayesian Regularization employs a more systematic optimization process. It significantly improves the model's generalization performance and predictive stability, fundamentally ensuring its practicality and reliability for engineering decision-making. In summary, given the task of modeling the mechanical behavior of concrete, which involves scarce data and stringent requirements for predictive robustness, the Bayesian Regularization algorithm achieves a better balance between accuracy and reliability, making it the appropriate choice for this study.

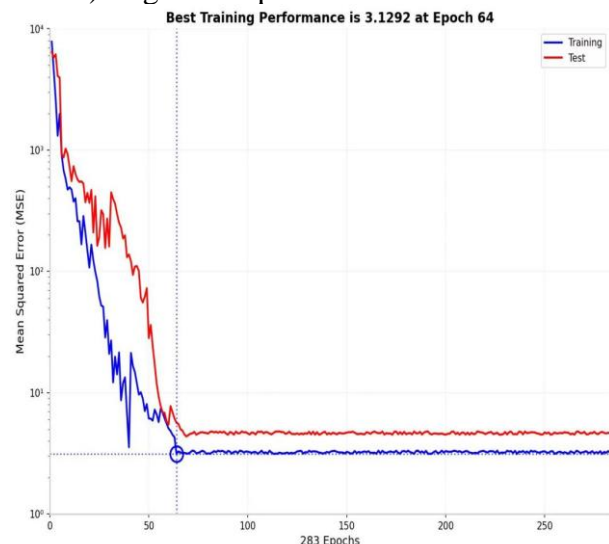
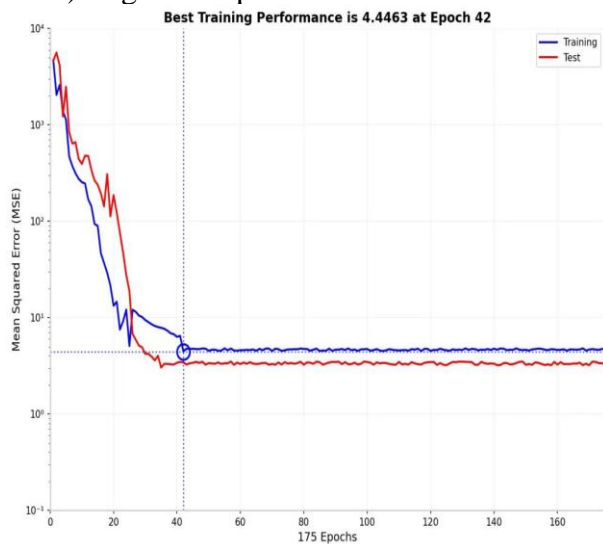
3.3 Data validation

The BP neural network learning model was constructed according to Figure 6. The output of this trained model was designed as the Load, F. The model was trained using the training dataset (80% of the total dataset). The results are shown in the corresponding Figure 7a and 7b.



a) Regression plot for the flexural beam

b) Regression plot for the shear beam



c) Training performance for the flexural beam

d) Training performance for the shear beam

Figure 7 – Performance of the BP neural network prediction model

The regression value (R-value) for the trained flexural model is 0.994, and for the trained shear model, it is 0.999. The Mean Squared Error (MSE) for the trained flexural model is 4.446, and for the trained shear model, it is 3.129. The remaining 20% of the dataset was applied to validate the trained model. The results are shown in the corresponding Figures 7c and 7d. The regression value

(R-value) for the validated flexural data is 0.996, and for the validated shear data, it is 0.998. The MSE for the validated flexural model is 2.632, and for the validated shear model, it is 5.430.

Based on the performance of the current models, the BP neural network models trained on both datasets exhibit high regression values (close to 1) and low Mean Squared Errors. Furthermore, the results from the training and testing phases are close. This demonstrates the high accuracy of the models. The models can predict the load applied to an RC beam based on the strain in the concrete. Consequently, they can be used for predicting the failure stage of reinforced concrete beams.

It is noteworthy that the high regression performance ($R > 0.99$) reported herein is derived from a limited sample size ($n=28$). Given the 80/20 split, the test set is statistically insufficient to capture potential process variability or noise. Thus, while the Bayesian-regularized BPNN demonstrates excellent fitting within the sampled domain, claims of its broad applicability should be tempered. The results primarily serve to establish a proof-of-concept within the specific experimental regime, necessitating future studies with expanded datasets to validate predictive robustness beyond the interpolation range.

4. Conclusion

1. Flexural failure in under-reinforced beams exhibits ductile characteristics. Experimental analysis shows that during the flexural failure of an under-reinforced beam (designed with a reinforcement ratio to ensure steel yields before concrete crushing), the tensile steel yields first. For instance, at a load of 60 kN, the steel strain reached 1500 $\mu\epsilon$. This is followed by the crushing of the concrete, forming a plastic hinge. The load-deflection curve shows a distinct yield plateau, where the deflection increased abruptly from 10.10 mm to 15.15 mm. This failure mode provides ductile warning, adhering to the “yield-before-failure” design principle for under-reinforced beams.

2. Shear failure demonstrates sudden, brittle characteristics. During tests, beams with short shear spans exhibited higher load-carrying capacity (up to 140 kN, 2.2 times that of the flexural beam) through “arch action”. However, failure occurred suddenly, characterized by a load increase from 120 kN to 140 kN accompanied by a sharp deflection jump of 4.75 mm and a rapid surge in steel strain. This constitutes a brittle, catastrophic failure mode that must be avoided in engineering practice.

3. The neural network model effectively predicts beam failure. The BP neural network model, based on the Bayesian Regularization algorithm, uses concrete strain as input and load as output. The model achieved high regression values, close to 1, for both training and testing (Flexural: 0.994, 0.995; Shear: 0.999, 0.998), along with low Mean Squared Errors. This confirms the model's high accuracy in predicting the load and identifying the failure stage of reinforced concrete beams, demonstrating its suitability for engineering applications.

Acknowledgments

This work was supported by the National Natural Science Foundation of China (Grant No. 52368051). The abovementioned funding sources and support are gratefully acknowledged.

Reference

- [1] B. Bakleh, G. Wardeh, H. Hasan, A. Jahami, and A. Formisano, “A Physically Based 1D Finite Element Framework for Long-Term Flexural Response of Reinforced Concrete Beams,” *CivilEng*, vol. 7, no. 1, p. 15, 2026, doi: 10.3390/civileng7010015.
- [2] I. I. Luchko and V. F. Lazar, “Evaluation of Stresses in Reinforced-Concrete Beam Elements, Their Strength, and Crack Resistance,” *Mater. Sci.*, vol. 38, no. 1, pp. 136–150, 2002, doi: 10.1023/A:1020145420154.
- [3] Z. Nuguzhinov *et al.*, “Stress Intensity Factor of Reinforced Concrete Beams in Bending,” *Buildings*, vol. 11, no. 7, p. 287, 2021, doi: 10.3390/buildings11070287.
- [4] P. L. Ng, J. Y. K. Lam, and A. K. H. Kwan, “Tension stiffening in concrete beams. Part 1: FE analysis,” *Proc. Inst. Civ. Eng. - Struct. Build.*, vol. 163, no. 1, pp. 19–28, 2010, doi: 10.1680/stbu.2009.163.1.19.
- [5] L. C. Hoang and M. P. Nielsen, “Continuous reinforces concrete beams: stress and stiffness estimates in the serviceability limit state,” in *BKM Serie R, Rapportør / Institut for Baerende Konstruktioner og Materialer, Danmarks Tekniske Universitet*, Lyngby, Denmark: Danmarks Tekniske Universitet, 1996, p. 42.

- [6] L. Y. Zhou and L. Qiao, "Ultimate Load Analysis of Reinforced Concrete Beam with Finite Element," *Adv. Mater. Res.*, vol. 243–249, pp. 1340–1345, 2011, doi: 10.4028/www.scientific.net/AMR.243-249.1340.
- [7] A. R. T. Wayghan and V. Sadeghian, "A Shear Hinge Model for Analysis of Reinforced Concrete Beams," *ACI Struct. J.*, vol. 118, no. 6, pp. 279–291, 2021, doi: 10.14359/51733001.
- [8] D. T. W. Looi, R. K. L. Su, and E. S. S. Lam, "A unified shear stress limit for reinforced concrete beam design," *HKIE Trans.*, vol. 22, no. 4, pp. 223–234, 2015, doi: 10.1080/1023697X.2015.1102654.
- [9] M. V. G. Silveira and R. A. D. Souza, "Analysis and design of reinforced concrete deep beams using the stress fields method," *Acta Sci. Technol.*, vol. 39, no. 5, p. 587, 2017, doi: 10.4025/actascitechnol.v39i5.28409.
- [10] A. Jierula, X. Li, W. Wang, H. Niyazi, and S. Wang, "Experimental study on mechanical properties of polypropylene fiber foamed concrete after exposure to high temperatures," *Case Stud. Constr. Mater.*, vol. 24, p. e05966, 2026, doi: 10.1016/j.cscm.2026.e05966.
- [11] A. Jierula, S. Ding, H. Liu, and B. Yang, "Damage Evolution in Different Reinforcement Configurations during Four-Point Bending: Acoustic Emission Analysis Using K-means Clustering," *J. Nondestruct. Eval.*, vol. 45, no. 1, p. 40, 2026, doi: 10.1007/s10921-026-01333-x.
- [12] A. Jierula, T.-M. Oh, S. Wang, J.-H. Lee, H. Kim, and J.-W. Lee, "Detection of damage locations and damage steps in pile foundations using acoustic emissions with deep learning technology," *Front. Struct. Civ. Eng.*, vol. 15, no. 2, pp. 318–332, 2021, doi: 10.1007/s11709-021-0715-y.
- [13] A. Jierula, S. Wang, T.-M. Oh, J.-W. Lee, and J. H. Lee, "Detection of source locations in RC columns using machine learning with acoustic emission data," *Eng. Struct.*, vol. 246, p. 112992, 2021, doi: 10.1016/j.engstruct.2021.112992.

Information about authors:

Abudusaimaiti Kali – MSc; 1) College of Civil Engineering and Architecture, Xinjiang University, Urumqi, China; 2) Xinjiang Key Laboratory of Building Structure and Earthquake Resistance, Xinjiang University, Urumqi, China; abdusmt@xju.edu.cn

Zihao Wang – Bachelor Student; 1) College of Civil Engineering and Architecture, Xinjiang University, Urumqi, China; 2) Xinjiang Key Laboratory of Building Structure and Earthquake Resistance, Xinjiang University, Urumqi, China; 880711@stu.xju.edu.cn

Alipujiang Jierula – PhD; 1) College of Civil Engineering and Architecture, Xinjiang University, Urumqi, China; 2) Xinjiang Key Laboratory of Building Structure and Earthquake Resistance, Xinjiang University, Urumqi, China; alpj@xju.edu.cn

Author Contributions:

Abudusaimaiti Kali – methodology, testing, modeling, analysis, interpretation, editing.

Zihao Wang – data collection, testing, analysis, visualization, drafting, editing.

Alipujiang Jierula – concept, methodology, resources, testing, analysis, interpretation, editing, funding acquisition.

Conflict of Interest: The authors declare no conflict of interest.

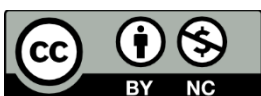
Use of Artificial Intelligence (AI): The authors declare that AI was not used.

Received: 02.05.2026

Revised: 20.06.2026

Accepted: 25.06.2026

Published: 26.06.2026



Copyright: © 2026 by the authors. Licensee Technobius, LLP, Astana, Republic of Kazakhstan. This article is an open access article distributed under the terms and conditions of the Creative Commons Attribution (CC BY-NC 4.0) license (<https://creativecommons.org/licenses/by-nc/4.0/>).